Particle density stratification in transient sedimentation

S. L. Dance* and M. R. Maxey
Division of Applied Mathematics, Brown University, Providence, Rhode Island 02912, USA
(Received 16 March 2003; published 10 September 2003)

Theoretical predictions for the scaling of particle velocity fluctuations with container size in homogeneous Stokes suspensions are not consistent with experimental observations. Several explanations have been advanced, including the formation of stratification in bounded systems, such as those used in experiments. Numerical simulations of transient Stokes sedimentation in bounded cells are presented here for several cell sizes. The simulated cells have top and bottom wall boundaries and periodic boundaries in the horizontal. Throughout the course of the simulations the number and distribution of particles in the cell evolve, with impacts on the bulk mean particle velocity, velocity fluctuations, and particle density gradient. Initially the sedimentation follows the classical description, with a sharp front and uniform particle concentration below, but this is not sustained. A layer of higher particle concentration develops below the front. This is unstable and there is a large-scale overturning of the fluid. As a consequence, there is a redistribution of the particles, leaving behind a mass loading of the particles, which is stably stratified (subject to small density fluctuations between horizontal levels). The mean velocity and fluctuations of the particles initially grow and then decay once stable stratification has developed.

DOI: 10.1103/PhysRevE.68.031403 PACS number(s): 82.70.Kj, 47.15.Gf, 83.85.Pt

I. INTRODUCTION

In Stokes flow, an isolated sphere falls steadily through a suspending liquid, at a terminal velocity determined by a balance between the weight of the particle and the drag on it. In a suspension of many particles, the velocity of each particle is determined by the instantaneous configuration of its neighbors. For example, isolated clusters of particles settle more rapidly, whereas on average there is a hindered settling effect. Such interactions cause fluctuations in particle velocity, which lead to dispersion of the particles, in addition to a net sedimentation flow. The scaling of these fluctuations in Stokes sedimentation has been a source of controversy (for a review see Ramaswamy [1]). Theoretical work [2] gave a scaling of the particle velocity fluctuations that increased with the size of the sedimentation vessel. This was supported by results from numerical simulations with fully periodic boundary conditions [3,4]. However, the theory proved to be inconsistent with experimental data (for example, Refs. [5–8]). According to Segrè *et al.* [7,8] the fluctuation levels saturate for cells larger than a certain correlation length, which scales as $\sim a\phi^{-1/3}$. (Here a is the particle radius and ϕ is the volume fraction.) For smaller cells, the fluctuations exhibit a linear dependence on cell size.

The theoretical scaling of the velocity fluctuations is derived from an idealized model that differs from experimental systems in a number of respects. The challenge is to identify the dominant physical mechanism that should be included. Several authors have examined the assumptions of the theory and proposed physical mechanisms to explain the differences between theory and experiment. Koch and Shaqfeh [9] considered a Debye-like screening, where the particles arrange themselves locally in configurations that exactly cancel the divergence in the fluctuations. This leads to a correlation length inconsistent with the findings of Segrè *et al.* Nonlinear advection-diffusion mechanisms [10,11] have been put forward, which rely on assumptions about the form of the diffusivity. Brenner's work on side walls [12] showed that they mollify but do not eliminate the divergence in fluctuations with container size. Ladd [13] carried out simulations in cells bounded by walls on all sides, and found that fluctuation levels did indeed saturate for sufficiently wide cells. Luke [14] showed that the presence of a stable concentration gradient in a suspension will act to damp out particle density fluctuations, and hence velocity fluctuations. Recently, these ideas have been developed further [15].

The evolution of the particle density distribution in a monodisperse suspension is described by a classical theory [16]. In this theory, a dense layer of particles forms at the bottom of the cell with a smooth transition to a layer of uniform density above. The density of this uniform layer is matched to the initial value. Located above this is the sedimentation front that can either be a sharp front under a layer of nearly zero void fraction or a diffuse front where the density gradient spans a significant portion of the cell. The behavior of the front is determined according to the Peclet number (defined as the ratio of hydrodynamic to Brownian diffusivity). In the high Peclet number limit, where Brownian motion is negligible, the front is expected to be sharp: the theory predicts diffuse fronts for smaller Peclet numbers, which might occur if the suspension is polydisperse. There are only limited experimental measurements of the evolution of the particle density profile available [17–19] and very little work has considered density profiles from simulations [13,15].

The purpose of this work is to carry out numerical simulations to determine whether stable stratification will develop in a sedimentation cell and to consider the impact of such a stably stratified particle concentration on the particle velocity

*Present address: Department of Meteorology, University of Reading, Earley Gate, P.O. Box 243, Reading RG6 6BB, UK; electronic address: s.l.dance@reading.ac.uk

distribution. All particles in the simulations are identical rigid spheres. Fluid inertia, particle inertia, and Brownian motion are neglected. The computational domain is wall bounded in the vertical and has periodic boundary conditions in the horizontal. The results show that a concentration gradient does eventually form, independent of container width, following convective overturning within the cell. It is hoped that these surprising results will stimulate further experimental studies.

The paper is organized as follows. In Sec. II the simulation methods, parameters for the numerical experiments and statistics calculated in processing the data are described. Results are presented in Sec. III. These include time series of volume fraction profiles and bulk statistics for particle velocities. Profiles of vertical particle velocity and local density fluctuations are also considered. A qualitative explanation of the results in terms of particle cluster dynamics is given. The effects of neglecting force-coupling method (FCM)-force-dipole terms in the simulations are considered in Sec. IV. We summarize the results and conclude in Sec. V.

II. SIMULATION METHODS AND PARAMETERS

A. The force coupling method

Simulations are carried out using the FCM. In this section a brief overview of the method is given. For further details, the reader is referred to the descriptions in Refs. [20–22].

The whole domain, including the particles, is treated as fluid. The fluid velocity field $\mathbf{u}(\mathbf{x},t)$ and pressure $p(\mathbf{x},t)$ satisfy the Stokes equations:

$$-\mu\nabla^2\mathbf{u}+\nabla p=\mathbf{f}, \tag{1}$$

$$\nabla\cdot\mathbf{u}=0, \tag{2}$$

where μ is the dynamic viscosity of the fluid. The fluid momentum equation (1) is augmented with a source term $\mathbf{f}(\mathbf{x},t)$, which approximates the effect of the particles on the flow, using the FCM-multipole terms:

$$f_i(\mathbf{x},t)=\sum_{n=1}^{N} F_i^{(n)}\Delta(\mathbf{x}-\mathbf{Y}^{(n)}(t))+G_{ij}^{(n)}\frac{\partial\Theta}{\partial x_j}(\mathbf{x}-\mathbf{Y}^{(n)}(t)). \tag{3}$$

The sum is over all the particles in the system, the nth particle being located at $\mathbf{Y}^{(n)}(t)$. The functions $\Delta(\mathbf{x})$ and $\Theta(\mathbf{x})$ are spherically symmetric Gaussian functions:

$$\Delta(\mathbf{x})=\frac{1}{(2\pi\sigma_\Delta^2)^{3/2}}\exp\left(\frac{-\mathbf{x}^2}{2\sigma_{\Delta,n}^2}\right), \tag{4}$$

$$\Theta(\mathbf{x})=\frac{1}{(2\pi\sigma_\Theta^2)^{3/2}}\exp\left(\frac{-\mathbf{x}^2}{2\sigma_{\Theta,n}^2}\right), \tag{5}$$

where σ_Δ and σ_Θ are length scales related to the particle radius a. Their values are calculated by matching FCM particle velocities to those obtained with exact solutions. This results in $\sigma_\Delta=a/\pi^{1/2}$ and $\sigma_\Theta=a/(36\pi)^{1/6}$. For details of these calculations, see Refs. [20,21]. The force-monopole strength $\mathbf{F}^{(n)}$ is equal to the hydrodynamic drag on the nth particle. Typically, this is equal to the buoyancy adjusted weight of the particle, minus the particle inertia:

$$\mathbf{F}^{(n)}=(m_p-m_f)\left(\mathbf{g}-\frac{d\mathbf{V}^{(n)}}{dt}\right).$$

In this work particle inertia is neglected. This is appropriate for sedimenting suspensions where the effect of gravitational acceleration is much larger than accelerations in the fluid.

Dipole terms $G_{ij}^{(n)}$ are not included for now so as to make computations feasible in reasonable time for large numbers of particles. Estimating the degree of error introduced is discussed in Sec. IV. In the context of the present problem, there are quantitative but not qualitative differences. For details of the calculation of this term, the reader is referred to Dance and Maxey [23] and Lomholt and Maxey [21].

Initial positions for each particle are prescribed via a random seeding. Particle positions then evolve as

$$\frac{dY_i^{(n)}}{dt}=V_i^{(n)}. \tag{6}$$

The particle velocities are computed as a local average of the fluid velocity:

$$V_i^{(n)}(t)=\int u_i(\mathbf{x},t)\Delta(\mathbf{x}-\mathbf{Y}^{(n)}(t))d^3\mathbf{x}. \tag{7}$$

With this definition for the velocity, there is a consistent balance between the rate of work done by the particulate phase and viscous dissipation of kinetic energy by the fluid [20].

Further details and extensions of the model are documented [21,22]. The model has been used for particulate flows in a number of geometries, including suspension flows [24].

B. Numerical solution of the FCM equations

The FCM equations are solved in a domain with wall (no-slip) boundaries in the vertical and periodic boundaries in the horizontal. A mixed Fourier/spectral element discretization is used with the Uzawa algorithm to solve for the flow. The code is described in Appendix A. Particles are advected using a third-order Adams-Bashforth scheme. A repulsive potential force barrier is imposed for interparticle and particle-wall collisions. The form of this force and its effects on the bulk flow and microstructure are discussed in another paper [25].

C. Experimental parameters

Several different size sedimentation cells are used for comparison. The height $H=50a$ or $100a$. The width L varies between $15a$ and $80a$. The flow is randomly seeded with particles as the initial conditions and the initial volume fraction is fixed at 11.6%. The number of particles in the cell is denoted by N. The particles are all identical spheres, with

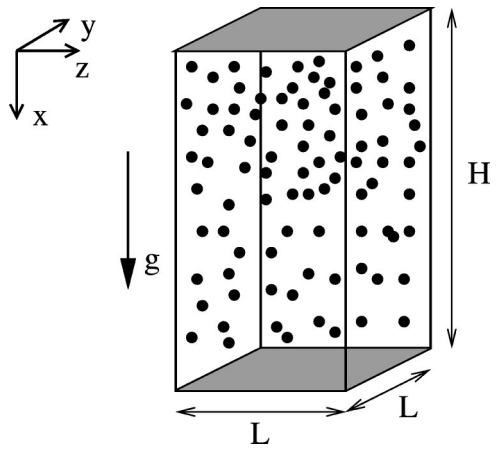

FIG. 1. The geometry for the suspension simulations.

radii $a=1.0$. An illustration of the geometry is given in Fig. 1 and the parameters for each box size are given in Table I.

The force on each particle is set as $6\pi\mu a$, corresponding to a Stokes settling velocity of 1.0 in an infinite fluid. This sets the Stokes time scale in the domain, $t_S=a/V_S=1.0$. In this geometry, the velocity of a single particle actually varies with height in the box, with a maximum value at the midplane, due to the no-slip conditions on the particle walls. The value also depends on the width of the box, due to the periodic boundary conditions in the horizontal.

As the particles reach the bottom of the box, they are removed. Whilst this does not reproduce experimental conditions exactly, it allows the simplifying assumption of a fixed length scale H for the effective height of the cell, and is computationally convenient. This is discussed further in Sec. V.

D. Statistics

A bulk region B of the domain is defined as $0\leqslant y,z\leqslant L$, and $10\leqslant x\leqslant 40$ or $10\leqslant x\leqslant 90$, for $H=50$ or 100, respectively. The choice of the bulk region of flow corresponds to the region where the velocity of a single particle falling through the box is at least 95% of its maximum value. The reader may find it useful to think of the bulk flow region as that where the influence of the no-slip condition on the top and bottom walls is less significant.

An overbar denotes a spatial average over the bulk region of a continuous function, $g(\mathbf{x},t)$:

$$\overline{g}(t)=\frac{1}{\Omega_B}\int_B g(\mathbf{x},t)d\mathbf{x}, \tag{8}$$

where Ω_B is the volume of the bulk region.

For some particle attributes, such as $g^{(n)}$, say, it is more appropriate to calculate the mean over all the particles located within the bulk region, this is denoted with angle brackets:

$$\langle g(t)\rangle=\frac{1}{N_B(t)}\sum_{\{n:\mathbf{Y}^{(n)}\in B\}} g^{(n)}, \tag{9}$$

TABLE I. Simulation parameters.

	N	L/a	H/a	Resolution
Parameter set *A*	313	15.0	50.0	$100\times24\times24$
Parameter set *B*	1250	30.0	50.0	$100\times48\times48$
Parameter set *C*	5000	60.0	50.0	$100\times96\times96$
Parameter set *D*	8889	80.0	50.0	$100\times128\times128$
Parameter set *E*	10000	60.0	100.0	$199\times96\times96$

where N_B is the number of particles within the bulk region at time t.

The Dirichlet boundaries at the top and bottom of the sedimentation cell introduce vertical inhomogeneity in the flow. However, each horizontal plane is assumed to be statistically homogeneous, thus it makes sense to consider horizontally averaged statistics. The vertical profile of the local volume fraction is defined as

$$\hat{\phi}(x,t)=\frac{1}{L^2}\int\sum_{n=1}^{N}\Omega_p\Delta(\mathbf{x}-\mathbf{Y}^{(n)}(t))dydz, \tag{10}$$

where the sum is over the N particles in the domain at time t and Ω_p is the volume of a particle. Δ is the particle distribution envelope, defined in Eq. (4). The integral is taken over the whole horizontal plane.

Horizontally averaged profiles of vertical particle velocity are defined as

$$\hat{V}(x,t)=\frac{\frac{1}{L^2}\int\sum_{n=1}^{N}V^{(n)}\Delta(\mathbf{x}-\mathbf{Y}^{(n)}(t))dydz}{\hat{\phi}}, \tag{11}$$

where the sum is over the N particles in the domain at time t.

III. RESULTS

In Fig. 2(a) time series of the volume fraction profile $\hat{\phi}(x,t)$ [defined in Eq. (10)] is illustrated for parameter set *E*. Initially the seeding of particles is uniformly distributed in the bulk region with a particle depleted layer next to the top and bottom walls, since the particles may not overlap with the walls. The small fluctuations between horizontal levels are a consequence of the random seeding. At first, the volume fraction profile evolves according to the classical theory, with a dense layer forming at the bottom of the cell with a smooth transition to a layer of uniform density above, which is matched to the initial value. Located above this is a relatively sharp sedimentation front. However, when $t/t_S=30$–40 a dense layer develops, just below the sedimentation front, that has a much higher particle volume fraction than the fluid immediately below it. This is unstable and there is a large scale overturning of the fluid which leads to a redistribution of the particles. By $t/t_S=50$ this leaves behind it a stably stratified mass loading of the particles, subject to small statistical fluctuations in density between horizontal levels. The formation of locally dense layers or overhangs occurs again, but not as strongly, later in the simulation,

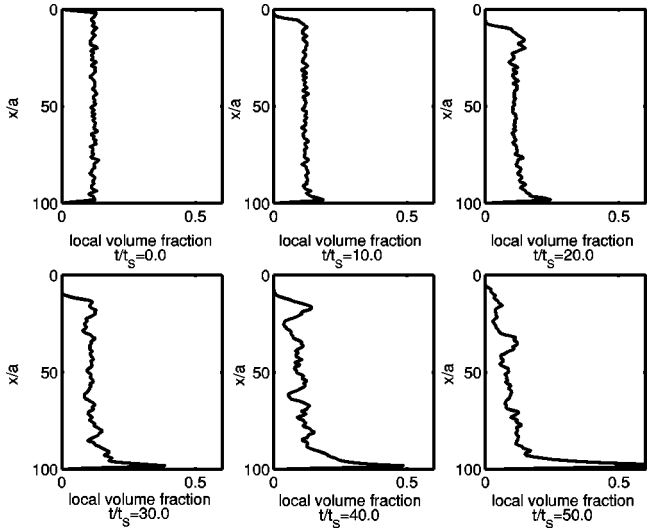

FIG. 2. A time series of the vertical profiles of the local volume fraction $\hat{\phi}$ for parameter set *E*.

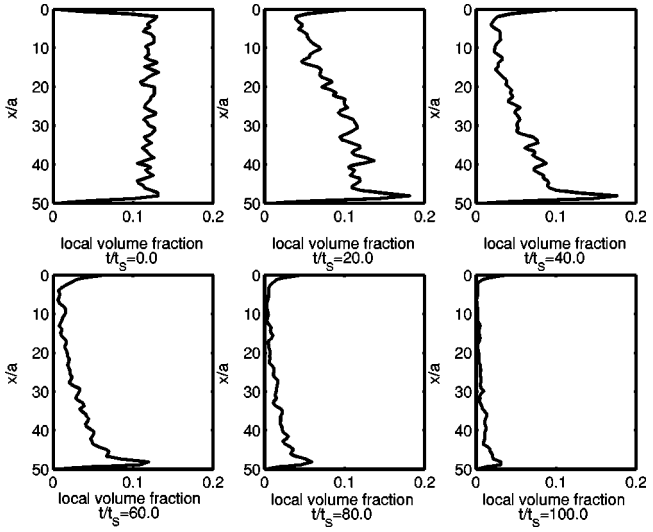

FIG. 3. A time series of the vertical profiles of the local volume fraction $\hat{\phi}$ for parameter set *C*.

lower down in the cell. The number of particles is large enough that statistical fluctuations in the density are small compared with the excess density in these overhangs. This suggests that convective overturning can develop, even if the initial density is uniform.

In Fig. 3 an example of a time series of the density profile, $\hat{\phi}(x,t)$, is shown for *C* (whose cell height is half that of *E*). Early on a similar overturning event occurs in the cell. Some particles recirculate and temporarily stick to the container lid. There is some evidence that this also occurs in other independent simulations, e.g., Fig. 9 of Ref. [15]. In the bulk region, a particle density concentration gradient soon develops, with a dense layer of particles just above the bottom wall. The gradient may be quantified by calculating the line of best fit in the bulk region. Using this measure, the largest gradient occurs between $20t_S$ and $30t_S$. Subsequently, the gradient decreases, but the stable stratification persists as particles settle out of the system and the bulk volume fraction decreases.

The volume fraction profile evolves in a similar way for each set of parameters with the same cell height (A,B,C,D). An illustration comparing a snapshot of the profile for each set of parameters is given in Fig. 4. The solid lines represent the function $\hat{\phi}(x,20t_S)$ for one realization. The wider cell sizes show less statistical variation from horizontal level to horizontal level, since there are a larger number of particles in the system. The dashed lines are lines of best fit to the data in the bulk region. The gradient of ϕ with respect to x corresponding to this line are, for each case, *A* 0.0004, *B* 0.0012, *C* 0.0024, *D* 0.0018.

During the course of each simulation, the number of particles in the bulk region (defined in Sec. II D) decreases as the particles settle out of the system. The initial (ϕ_0) and final (ϕ_{100}) volume fractions in the bulk region are given in Table II. The initial distribution of particles is uniform throughout the box, with the caveat that they do not overlap with each other or the container walls. Thus there is a particle depleted layer next to the top and bottom walls, which is compensated for by a slightly larger number density of particles in the bulk of the fluid. As a result, the initial volume fraction in the bulk region is slightly higher than the initial volume fraction for the whole cell. For parameter sets *A*, *B*, *C*, and *D*, after $100t_S$ there are very few particles left in the bulk region. For parameter set *E* (the tall cell), there are slightly less than half of the initial number of particles left in the system. Furthermore, ϕ_{100} for *E* is similar in value to ϕ_{50} for *C*. The difference in volume fraction between *C* and *E* after $100t_S$ might be explained as follows. The mean settling velocities in each case are similar (see Fig. 5 and associated remarks below), so particle flux rates are also similar. Thus, cell *E*, which is twice as tall as cell *C*, contains twice as many particles as cell *C* at initial time, and therefore takes approximately twice as long for all the particles to settle out. Indeed, if time is scaled by H/V_S, the evolution of bulk volume fraction in cases *C* and *E* is approximately the same.

The bulk mean particle velocity, $\langle V(t)\rangle$, is defined as the average over all the particles within the bulk region [see Eq. (9)]. A plot of $\langle V(t)\rangle$ is given in Fig. 5. Each symbol represents a time average over $10t_S$, and an average over several realizations in the case of parameter sets *A* and *B*. The error bars represent the statistical error as the standard deviation of the mean [26], and thus take into account the number of particles in each calculation.

Each set of simulation parameters gives similar bulk mean velocities as a function of time. There does not appear to be a systematic dependence of the mean velocity on the box size, consistent with theoretical expectations. The spread of the data is comparable to the typical uncertainty reported in experiments (e.g., Nicolai *et al.* [27] have an uncertainty of ± 0.1 for the nondimensional mean vertical velocity at volume fractions of 0.05 and 0.1).

According to the Richardson-Zaki empirical law [28],

$$\langle V\rangle = V_S(1-\phi)^n,$$

with an exponent of 5, the expected initial bulk mean particle vertical velocity is $0.53V_S$, corresponding to $\phi_0 = 0.12$. As

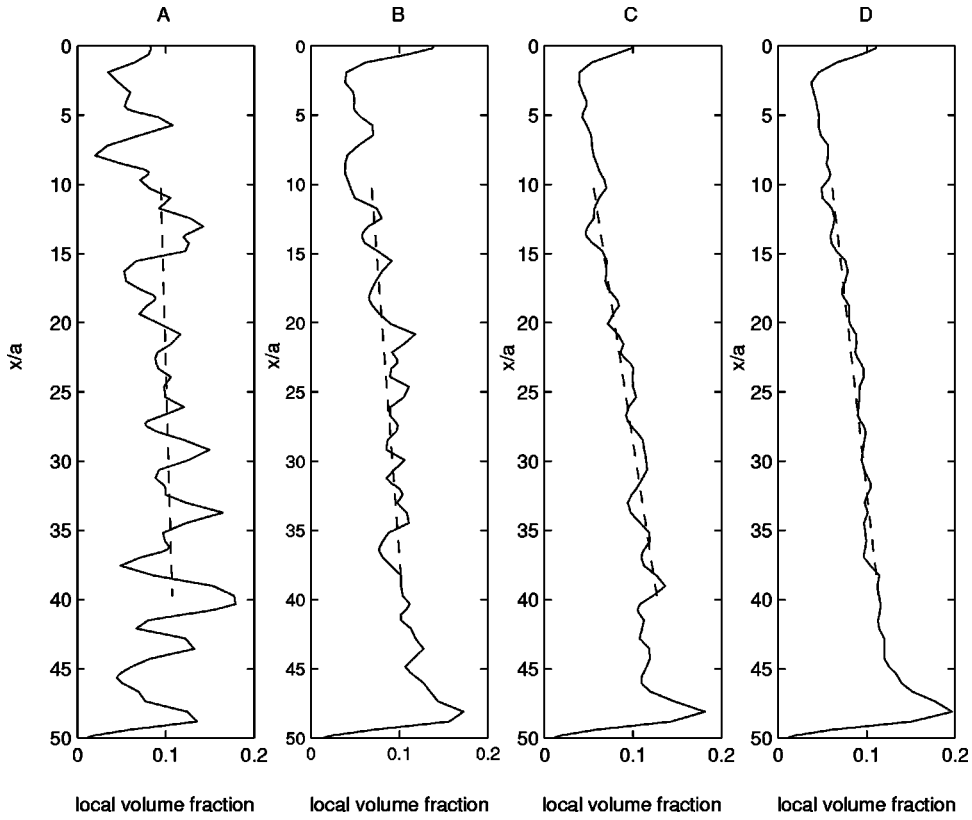

FIG. 4. Comparison of local volume fraction profiles at $t=20t_S$: $\hat{\phi}(x,20t_S)$ −; line of best fit to data in the bulk region - -.

the number of particles in the bulk region decreased, we would expect a steady increase in velocity, culminating with $0.95V_S$ at $t=100t_S$ and a nominal volume fraction of 0.01. For each simulation an initial velocity of a similar size to the Richardson-Zaki prediction is indeed observed. For *A*, *B*, *C*, and *D* the mean velocities increase during the period $0 \leqslant t/t_S \leqslant 40$, and the cells are ordered by bulk mean velocity magnitude as $A<B<C\sim D$. This period of gradual increase is followed by a jump in vertical velocity. After this event, the ordering of the cells by magnitude of bulk mean velocity is reversed: $D<C<B<A$. The peak in bulk mean settling velocity is later for E. Subsequently, the mean velocities decrease, even though the volume fraction in the domain is decreasing. Similarly, Guazzelli's experimental data [29] also show an initial increase followed by a decrease in the mean settling velocity.

In Fig. 6 the bulk rms vertical velocity fluctuations are plotted. Each symbol represents a time average over $10t_S$ and an average over several realization for experiments *A* and *B*. Surprisingly, there is no systematic dependence of the velocity fluctuations on container size. For $20t_S \leqslant t \leqslant 30t_S$, cell *A* exhibits the largest relative fluctuations. Comparing with Fig. 4 we see that cell *A* also has the largest density variations between horizontal levels at this time. A number of factors may be relevant here.

(1) The narrow cell has fewer particles in any horizontal layer, thus individual particles or particle clusters may have more effect.

(2) The periodic boundary conditions mean that any up or down flow must fit within this length scale. Fewer swirls or

TABLE II. Bulk region volume fraction statistics at $t=0$ and $t=100t_S$.

	ϕ_0	ϕ_{100}
Parameter set *A*	0.124	0.006
Parameter set *B*	0.120	0.006
Parameter set *C*	0.120	0.006
Parameter set *D*	0.120	0.004
Parameter set *E*	0.119	0.049

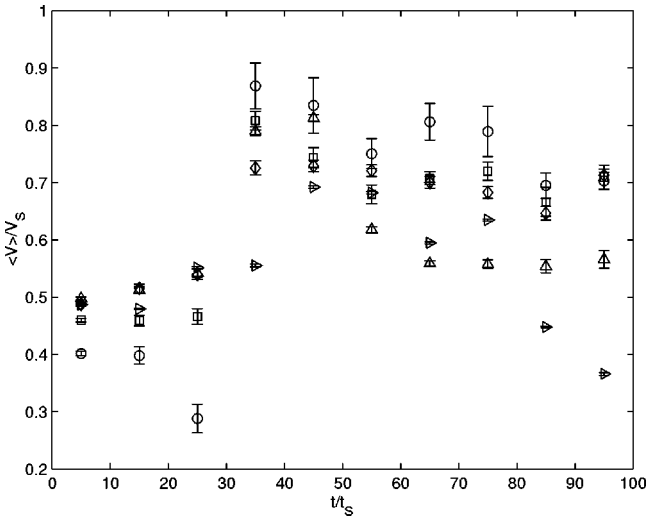

FIG. 5. Bulk mean settling velocity vs time. Symbols: ○, parameter set *A*; □, parameter set *B*; ◇, parameter set *C*; △, parameter set *D*; ▷, parameter set *E*.

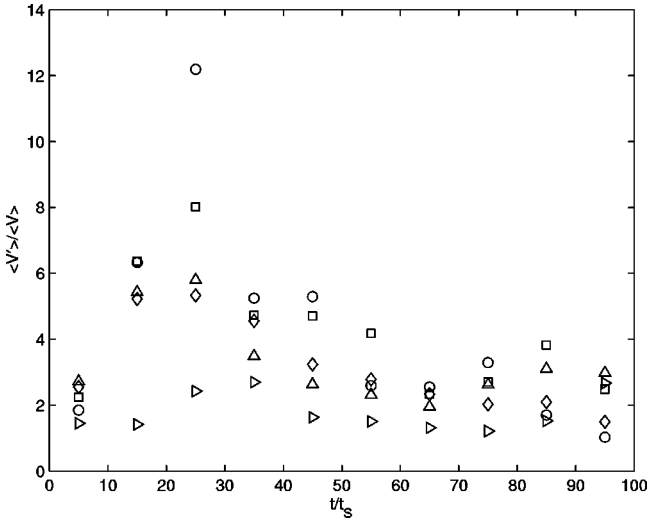

FIG. 6. Bulk mean vertical velocity fluctuations vs time. Symbols: ○, parameter set *A*; □, parameter set *B*; ◇, parameter set *C*; △, parameter set *D*; ▷, parameter set *E*.

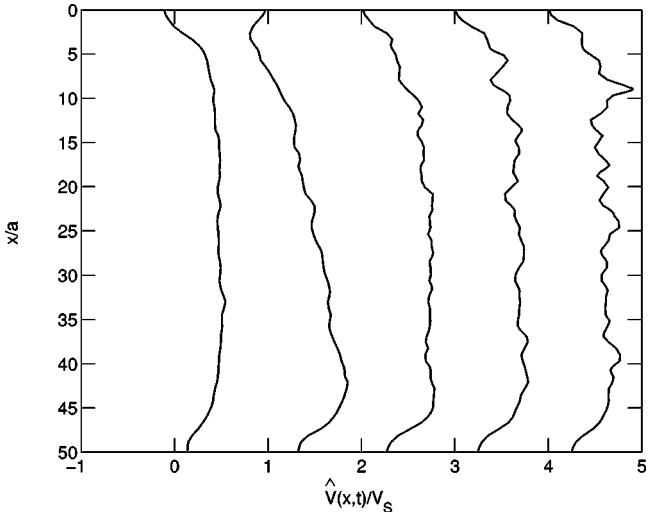

FIG. 7. Temporally averaged particle vertical velocity profiles $\hat{V}(x,t)$ for parameter set *C*, corresponding to times $0 \leqslant t \leqslant 10t_S$, $20t_S \leqslant t \leqslant 30t_S$, $40t_S \leqslant t \leqslant 50t_S$, $60t_S \leqslant t \leqslant 70t_S$, and $80t_S \leqslant t \leqslant 90t_S$.

eddies driven by local particle clustering can fit between the cell boundaries.

(3) Periodicity on this short scale may introduce long range correlations.

For each simulation, the relative magnitude of the velocity fluctuations grows initially and then decays. (An increase towards the end of the time period, evident for experiments *D* and *E* is probably a statistical artifact, since the number of particles remaining in the bulk region is very small at this time.) A time decay of fluctuation levels is predicted by Luke's theory [14]. This is also seen in some numerical simulations [13] and experiments of Refs. [19,29]. In experiments with thick cells [19], the decay continues up to the termination of data collection ($1000t_S$ or longer). In thinner cells, after an initial transient, the fluctuations decay to a uniform value.

The temporal decrease in velocity fluctuations is perhaps surprising if we consider the fluctuations as a function of volume fraction. In this system the volume fraction decreases with time as particles settle out of the cell. Thus an increase in fluctuation levels might be expected, based on experimental evidence for homogeneous systems. For example, results for a steady state fluidized bed [30] show an increase in fluctuation levels with decrease in ϕ.

In order to help understand these phenomena, consider profiles of vertical particle velocity, defined by Eq. (11). A series of these profiles is plotted for parameter set *C* in Fig. 7 and parameter set *E* in Fig. 8. Each profile plotted is averaged over a period of $10t_S$. The zero line for each profile is offset by an integer, for clarity. The profiles are constructed from particle data, which is distributed onto the computational grid using a Gaussian envelope. The profiles do not go exactly to zero at the upper and lower walls if there is a particle (or particles) near the walls with a nonzero velocity. This happens most often at the bottom wall where there is a weight of particles pressing down from above.

At first, the horizontally averaged particle velocities are uniform in the bulk region, with a decay at the walls due to the boundary conditions. At early times, the flow adjusts to the distribution of particles. Towards the top of the box, the return flow of liquid caused by the conservation of volume constraint sweeps some particles upwards. As the flow becomes organized, the mean particle velocity on each level again becomes positive. The velocities are approximately uniform in the bulk region of flow, with the velocities higher near the front.

Comparing Fig. 5 with Fig. 7 it is evident that the large jump in bulk mean vertical velocity corresponds to a change in profile character. To start with, the horizontally averaged

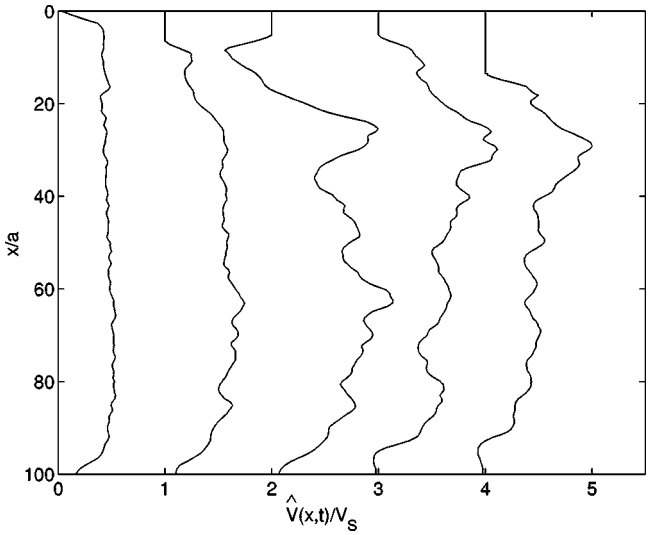

FIG. 8. Temporally averaged particle vertical velocity profiles $\hat{V}(x,t)$ for parameter set *E*, corresponding to times $0 \leqslant t \leqslant 10t_S$, $20t_S \leqslant t \leqslant 30t_S$, $40t_S \leqslant t \leqslant 50t_S$, $60t_S \leqslant t \leqslant 70t_S$, and $80t_S \leqslant t \leqslant 90t_S$.

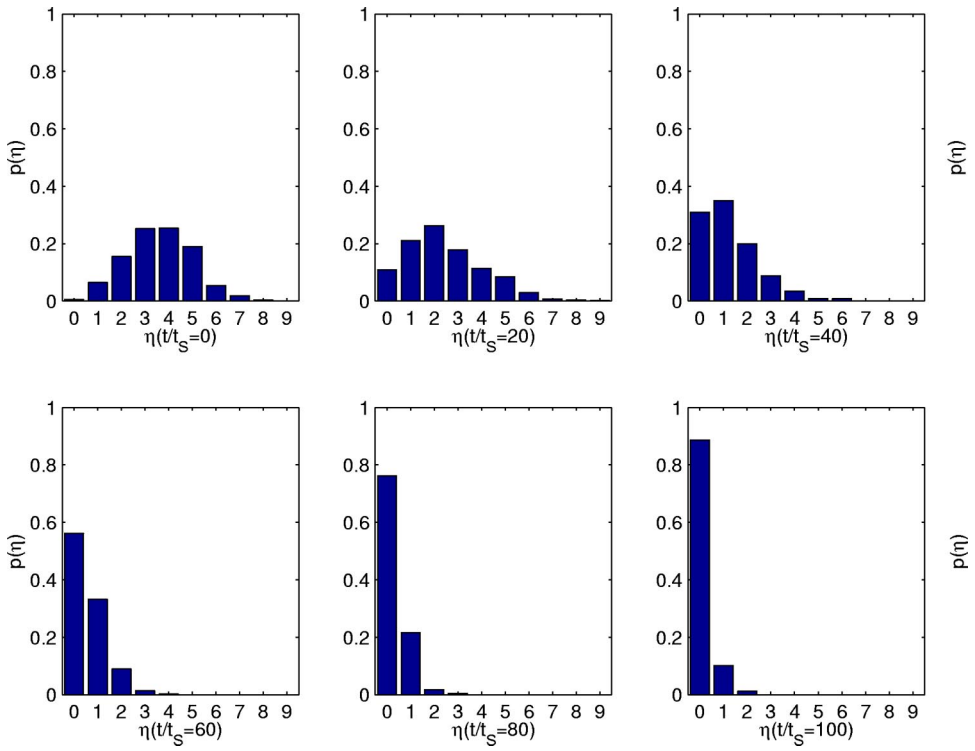

FIG. 9. A time series of the p.d.f.s for η for parameter set *C*.

particle velocity was upward at some levels, and then there is a transition to a situation in which the horizontally averaged particle velocities are all downwards. In other words, the initial increase in the bulk mean velocity corresponds to a reorganization of the flow and particle redistribution. Subsequently, the bulk mean velocity decreases. This is attributed to an increase in particle number density below the bulk region, which creates a blockage effect, and slows the particles down. The large velocity gradient evident in the profiles towards the bottom of the box supports this conclusion.

The local particle distribution is now considered, using a simple box-counting technique. The domain is divided into small cubes of side d and the number of particles in each cube, η, is counted. The probability density function (p.d.f.) of the number of particles in each cube at a given time t can then be calculated. An example of time series for the bulk region of flow with $d=5.0$, for parameter set *C*, is given in Fig. 9. The p.d.f. including the whole sedimentation cell is similar. Also, the p.d.f.s calculated with $d=4.0,6.0$ have the same features. At $t=0$ the p.d.f. corresponds to a uniform distribution of particles. Subsequently, the mean shifts to the left as fast moving clusters sediment out of the system. At the same time, the tail of the distribution becomes shorter, indicating the particle number fluctuations per box are decreasing. The particles become more dispersed and the distribution can no longer be considered uniform.

There are no experimental results available for the evolution of the three-dimensional distribution of particles. However, the p.d.f. of the two-dimensional particle distribution has been measured [31], by counting the number of particles in a test circle in illuminated regions of the flow, far from the side walls. The particle distribution evolved over time. Initially the distribution was Poisson (corresponding to uniformly distributed particles), but at later times, the particle number fluctuations decreased. These results are qualitatively similar to those from the simulations presented here.

This motivates the following tentative explanation of the results. Initially, the particles are uniformly distributed. Over a short initial period, the flow organizes, resulting in a new particle distribution. In particular, the Stokes flow structure encourages the formation of long-lived particle clusters. These experience less hydrodynamic drag than individual particles, and so sediment faster. The presence of many of these clusters leads to an increase in the bulk mean settling velocity. Analogously, such local density fluctuations increase the velocity fluctuations in the bulk flow. As clusters approach the bottom wall, the return flow acts to slow them down. The subsequent build up of particles arriving from above creates a more dense layer. This hindered settling, in turn, feeds back into higher sections of the cell. Hence a bulk stable stratification is created. There is also an associated decay of the bulk mean velocity. Gradually, the particles settle out of the system. Particle clusters selectively settle out faster than the mean, leaving behind a more dispersed distribution of particles. The growth in fluctuation levels continues for about $H/2V_S$, the time scale for density fluctuations to convect through half of the box. The subsequent decay in fluctuation levels is due to the increased mean interparticle spacing in the remaining particles. The bulk volume fraction (ϕ) decreases as the number of particles in the system is reduced. Consequently, the hindered settling phenomenon is less pronounced, allowing the concentration gradient $(d\phi/dx)$ to relax.

IV. DIPOLE EFFECTS

Cichocki *et al.* [32] carried out study of convergence of solutions for wall-bounded flow with multipole truncation

TABLE III. Parameters for the FCM-force-dipole test.

N, number of particles	1250
L/a, nondimensional width	30.0
H/a, nondimensional height	50.0
Resolution for FCM-monopole computations	$100\times48\times48$
Resolution for FCM-monopole and dipole computations	$199\times96\times96$

order for a classical multipole method. They found that the truncation order should be at least 2 and that there was a further improvement by using three terms, including additional terms seemed unnecessary. In this work, only one FCM-multipole term, the monopole, is employed. The use of the FCM-force dipole gives a chiefly local effect, which is most apparent for particles in shear flow [21,23]. For instance, the force dipole term prevents particle deformation during the close approach of another sphere.

The particle velocities computed with and without the dipole term for a system with parameters given in Table III are compared. Note that computations using the dipole term require a higher resolution grid. The tests were carried out by creating five randomly seeded arrangements of particles within the sedimentation cell and then comparing the particle velocities computed using each method.

The results indicated that there are small quantitative differences for the velocities of individual particles. Figure 10 shows the vertical velocity distribution for each method: Fig. 10(a) shows the computed velocity distribution using only the monopole term and Fig. 10(b) shows the distribution including the dipole. Using only the monopole term the distribution has mean 0.45 and standard deviation 0.52. The distribution calculated using the dipole term has mean 0.40 and standard deviation 0.39. Thus the p.d.f.s indicate that the use of a dipole term would make a small quantitative difference to the results, but a qualitative change is not anticipated.

V. SUMMARY AND CONCLUSIONS

Transient settling through a cell with top and bottom walls and periodic boundary conditions in the horizontal has been considered. Throughout the course of the simulations the number and distribution of particles in the cell evolved, with impacts on the bulk mean particle velocity, velocity fluctuations, and particle density gradient. Initially the sedimentation followed the classical description, with a sharp front and uniform particle concentration below, but this was not sustained. A layer of higher particle concentration developed below the front. This was unstable and there was a large-scale overturning of the fluid. As a consequence, there was a redistribution of the particles, leaving behind a mass loading of the particles that was stably stratified (subject to small density fluctuations between horizontal levels). The formation of locally dense layers or overhangs occurred again, but not as strongly, later in the simulation, lower down in the cell. The mean particle velocity and fluctuations were not constant in time, but grew whilst the flow became organized and then decayed for the rest of the experiment. The formation and differential settling of particle clusters appeared to be the key to understanding these phenomena.

In this light, we may reconsider the role of walls in screening velocity fluctuations in suspensions. The presence of a bottom wall enables large positive density fluctuations (particle clusters) to settle out, i.e., the wall acts as a sink for fluctuations. In simulations with periodic boundary conditions, these inhomogeneities are reintroduced at the top as they leave the bottom of the cell. Thus periodic boundaries prevent the particle distribution from evolving as it would in an experiment.

The data obtained in experiments, such as those of Segrè

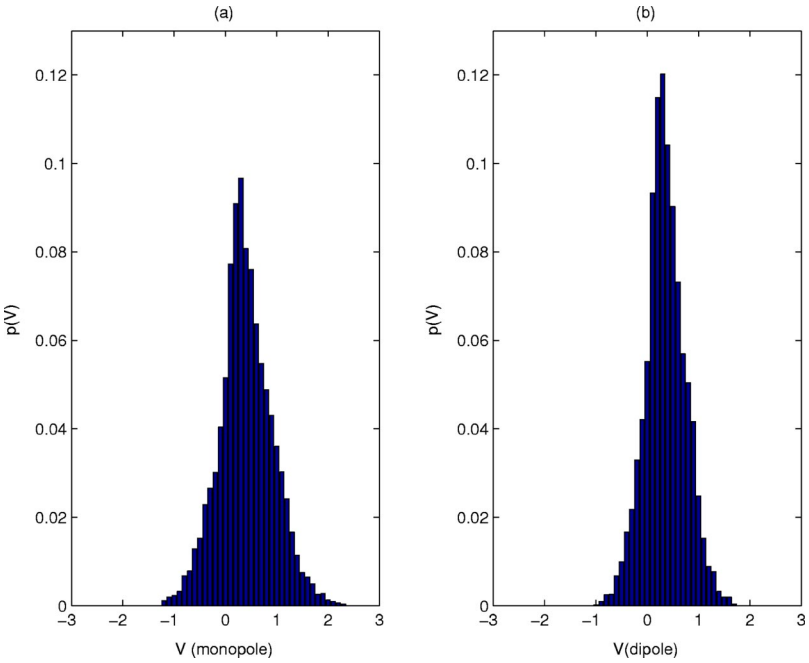

FIG. 10. P.d.f.s of the vertical velocities using one or two FCM-multipole terms.

et al. and Nicolai *et al.*, are typically taken some time after the cessation of mechanical mixing and the onset of settling, in order to allow the transient effects of mixing to die away. The simulation results would seem to indicate that in this transient period, the distribution of particles evolves, via differential settling of clusters, to a modified microstructure where the mean interparticle spacing is less than that would be expected for a uniform distribution of particles. What would appear to be needed now is careful experimental measurements of the evolution of the microstructure. Unfortunately, it is very difficult to measure the local particle distribution in three dimensions, although perhaps further measurements in two dimensions, such as those of Lei *et al.* [31], would provide insight.

A systematic dependence of particle velocity fluctuations on the box width was not observed. An explanatory hypothesis is that the side walls may have a role to play in changing the particle distribution. Typically, experimental data [6–8] is taken in the center of the cell, where the shortest distance from a side wall is larger than $10a$. Thus, one might assume that side wall effects should be negligible. However, the flow around particles close to the wall is modified relative to the flow around particles in the bulk of the cell [12]. Geometrical constraints imply that close to the walls there is a particle-depleted layer. Thus the side walls introduce horizontal inhomogeneities into the system, which are not present in these simulations. Such inhomogeneities may drive secondary flows, e.g., intrinsic convection [33]. It would be interesting to consider the results of simulations with side, top, and bottom walls, and examine the statistics of local particle density fluctuations across the width of the cell.

During the simulations, particles were removed from the bottom of the container. In experiments, particles are allowed to settle and form a sediment layer on the bottom of the cell. The weight of descending particles makes refluidization of the sediment layer energetically unfavorable. (Viscous resuspension is more likely in the context of shear flow [34].) Thus the effective cell height is gradually reduced, effectively moving the bottom boundary condition upwards. In our simulations, the initial volume fraction was 11.6%, thus allowing the particles to remain in the cell might result in a total reduction in cell height of about 15–20 % by the end of the experiment. Using the time scales from our simulations, the average rate of growth of the sediment layer would be about $0.075V_S$. As noted in Sec. II, the removal of particles allows the simplifying assumption of a fixed effective height, as well as being computationally convenient. Particle removal will affect the dynamics, but it is not anticipated that this effect will be major. However, our results should be viewed in the context of the simulations actually made.

The FCM model formulation utilized only the first-order accurate FCM-multipole term. However, the model does generalize to higher-order multipoles. The use of higher-order terms is not expected to affect the results in a qualitative sense (see Sec. IV), although the quantitative values of individual particle velocities may be slightly changed in some cases.

Even though several realizations were carried out for the small size boxes, and the large boxes contained a lot of particles, it may still be the case that there are some statistical fluctuations in the data. We do not, however, believe that the trends in the data would be changed significantly by increasing the size of the ensemble of experiments.

ACKNOWLEDGMENTS

The authors are grateful to P. N. Segrè (NASA Marshall Space Flight Center) and G. E. Karniadakis (Brown University) for useful discussions and comments. The work was supported by DARPA-ATO. Computations were carried out at TCASCV, Brown University and Boston University's SCF.

APPENDIX: CODE DESCRIPTION

We wish to solve the Stokes equations

$$-\mu\nabla^2\mathbf{u}+\nabla p=\mathbf{f}, \tag{A1}$$

$$-\nabla\cdot\mathbf{u}=0, \tag{A2}$$

for velocity $\mathbf{u}=(u,v,w)$ and pressure p in a domain $(0,L_x)\times(0,L_y)\times(0,L_z)$, subject to homogeneous Dirichlet (no-slip) conditions on the channel walls,

$$\mathbf{u}(0,y,z)=\mathbf{u}(L_x,y,z)=0,$$

and periodic boundary conditions in the y and z directions:

$$\mathbf{u}(x,0,z)=\mathbf{u}(x,L_y,z) \qquad \forall(x,z)\in(0,L_x)\times(0,L_z),$$

$$\mathbf{u}(x,y,0)=\mathbf{u}(x,y,L_z) \qquad \forall(x,y)\in(0,L_x)\times(0,L_y).$$

A mixed Fourier spectral element method is used to solve for the flow. A comprehensive introduction to spectral element methods as applied to computational fluid dynamics is given by Karniadakis and Sherwin [35].

Since the geometry is periodic in the wall-parallel directions, the velocity, pressure, and forcing may be written in the Fourier series representations:

$$\mathbf{u}(x,y,z)=\sum_{k,l}\hat{\mathbf{u}}(x,k,l)e^{i(\beta_y ky+\beta_z lz)},$$

$$p(x,y,z)=\sum_{k,l}\hat{p}(x,k,l)e^{i(\beta_y ky+\beta_z lz)},$$

$$\mathbf{f}(x,y,z)=\sum_{k,l}\hat{\mathbf{f}}(x,k,l)e^{i(\beta_y ky+\beta_z lz)},$$

where $\beta_y=2\pi/L_y$ and $\beta_z=2\pi/L_z$. For simplicity of notation, we restrict the rest of this description to the case where $L_y=L_z$ and write $\beta=\beta_y=\beta_z$. The algorithm is easily generalized to the case of $L_y\neq L_z$, as indeed it is in the code.

In practice, this transformation is discretized by truncation of the Fourier series. The efficient fast Fourier transform (FFT) can be used to carry out the transformation between physical and spectral space. The Fourier series transformation reduces the Stokes equations to a series of decoupled problems where we treat the wave numbers as parameters:

$$-\mu\left(\frac{d^2}{dx^2}-\lambda^2\right)\hat{u}+\frac{d\hat{p}}{dx}=\hat{f}^{(1)},$$

$$-\mu\left(\frac{d^2}{dx^2}-\lambda^2\right)\hat{v}+i\beta k\hat{p}=\hat{f}^{(2)},$$

$$-\mu\left(\frac{d^2}{dx^2}-\lambda^2\right)\hat{w}+i\beta l\hat{p}=\hat{f}^{(3)},$$

$$-\left(\frac{d\hat{u}}{dx}+i\beta k\hat{v}+i\beta l\hat{w}\right)=0,$$

with $\lambda^2=\beta^2(k^2+l^2)$.

The equivalent weak form is as follows. Find $(\hat{\mathbf{u}},\hat{p})$ in $X\times M$ such that

$$\mu\left\{\left(\frac{d\hat{u}}{dx},\frac{d\phi}{dx}\right)+\lambda^2(\hat{u},\phi)\right\}-\left(\hat{p},\frac{d\phi}{dx}\right)=(\hat{f}^{(1)},\phi),$$

$$\mu\left\{\left(\frac{d\hat{v}}{dx},\frac{d\phi}{dx}\right)+\lambda^2(\hat{v},\phi)\right\}+i\beta k(\hat{p},\phi)=(\hat{f}^{(2)},\phi),$$

$$\mu\left\{\left(\frac{d\hat{w}}{dx},\frac{d\phi}{dx}\right)+\lambda^2(\hat{w},\phi)\right\}+i\beta l(\hat{p},\phi)=(\hat{f}^{(3)},\phi),$$

for all $\phi\in X$, and

$$-\left(\frac{d\hat{u}}{dx}+i\beta k\hat{v}+i\beta l\hat{w},q\right)=0,$$

for all $q\in M$, where X and M are chosen to be

$$X=\mathcal{H}_0^1((0,L_x)),$$

$$M=\mathcal{L}_0^2((0,L_x))$$

so that the solutions are well posed [36]. Here $\mathcal{H}_0^1((0,L_x))$ is the space of all functions that are square integrable on $(0,L_x)$, whose derivatives are square integrable, and that satisfy the Dirichlet boundary conditions at $x=0,L_x$. $\mathcal{L}_0^2((0,L_x))$ is the space of square integrable functions on $(0,L_x)$ with zero average.

Following Rønquist [37], these equations are discretized using spectral elements. Due to the coupling between the velocity and pressure, they may not be discretized independently, to avoid spurious modes compatible subspaces must be chosen. For a discussion of the necessary conditions of compatibility see Canuto [38]. The domain $(0,L_x)$ is split into K equal elements, and the following subspaces that exclude parasitic modes are chosen:

$$X_h=\mathcal{H}_0^1((0,L_x))\cap\mathcal{P}_{N,K}((0,L_x))$$

$$M_h=\mathcal{L}_0^2((0,L_x))\cap\mathcal{P}_{N-2,K}((0,L_x)),$$

where $\mathcal{P}_{N-2,K}((0,L_x))$ is the space of polynomials of degree less than or equal to N restricted to the K elements. The choice of bases for these spaces corresponds to a discretization of the velocity using N Gauss-Lobatto-Legendre points on each element and the pressure using $N-2$ Gauss-Legendre points. In this way, we are able to impose the Dirichlet boundary conditions and preserve continuity of velocity between each element, but there are no boundary conditions on the pressure, and it may be discontinuous from element to element.

The Uzawa algorithm [35,39] is used to solve for the flow. The resulting matrix vector systems are solved using preconditioned conjugate gradient (PCG) methods. The preconditioner for the pressure equation is the diagonal Gauss-Legendre mass matrix (associated with the pressure discretization). The PCG residual corresponds to the discrete divergence of the velocity field, $-\mathbf{Du}$, and thus the specified convergence tolerance level reflects the degree to which the flow is incompressible. The spectrum of the preconditioned pressure operator is analyzed by Maday *et al.* [39]. In our implementation, for each given wave vector (k,l), the PCG pressure iteration typically converges within three iterations, as long as the spectral element resolution is high enough, which is consistent with Maday *et al.* results for semiperiodic problems.

The solution of the velocity equations involves the inversion of a Helmholtz operator. This is accomplished via PCG iteration with the inverse of the diagonal of the Helmholtz operator as preconditioner. This form of preconditioner is chosen since it is particularly easy to calculate. The condition number of the operator varies with wave number. In particle simulations, the lowest wave numbers require the most iterations for convergence.

Further details of the code and its validation (including spectral convergence tests) are given by Dance [40].

[1] S. Ramaswamy, Adv. Phys. **50**, 297 (2001).
[2] R.E. Caflisch and J.H.C. Luke, Phys. Fluids **28**, 759 (1985).
[3] A.J.C. Ladd, Phys. Rev. Lett. **76**, 1392 (1996).
[4] A.J.C. Ladd, Phys. Fluids **9**, 491 (1997).
[5] J.M. Ham and G.M. Homsy, Int. J. Multiphase Flow **14**, 533 (1988).
[6] H. Nicolai and E. Guazzelli, Phys. Fluids **7**, 12 (1995).
[7] P.N. Segrè, E. Herbolzheimer, and P.M. Chaikin, Phys. Rev. Lett. **79**, 2574 (1997).
[8] P.N. Segrè, F. Liu, P. Umbanhowar, and D.A. Weitz, Nature (London) **409**, 594 (2001).
[9] D.L. Koch and E.S.G. Shaqfeh, J. Fluid Mech. **224**, 275 (1991).
[10] A. Levine, S. Ramaswamy, E. Frey, and R. Bruinsma, Phys. Rev. Lett. **81**, 5944 (1998).
[11] P. Tong and B.J. Ackerson, Phys. Rev. E **58**, R6931 (1998).
[12] M.P. Brenner, Phys. Fluids **11**, 754 (1999).
[13] A.J.C. Ladd, Phys. Rev. Lett. **88**, 048301 (2002).

[14] J.H.C. Luke, Phys. Fluids **12**, 1619 (2000).
[15] P.J. Mucha, S.Y. Tee, D.A. Weitz, B.I. Shraiman, and M.P. Brenner (unpublished).
[16] W.B. Russel, D.A. Saville, and W.R. Schowalter, *Colloidal Dispersions* (Cambridge University Press, Cambridge, 1989).
[17] D. Chang, T. Lee, Y. Jang, M. Kim, and S. Lee, Powder Technol. **92**, 81 (1997).
[18] S. Lee, Y. Jang, C. Choi, and T. Lee, Phys. Fluids A **4**, 2601 (1992).
[19] S.Y. Tee, P.J. Mucha, L. Cipelletti, S. Manley, M.P. Brenner, P.N. Segre, and D.A. Weitz, Phys. Rev. Lett. **89**, 054501 (2002).
[20] M.R. Maxey and B.K. Patel, Int. J. Multiphase Flow **27**, 1603 (2001).
[21] S. Lomholt and M.R. Maxey, J. Comput. Phys. **184**, 381 (2003).
[22] S. Lomholt, Ph.D. thesis, Risø National Laboratory, 2002.
[23] S.L. Dance and M.R. Maxey, J. Comput. Phys. **189**, 212 (2003).
[24] E. Climent and M.R. Maxey, Int. J. Multiphase Flow **29**, 579 (2003).
[25] S.L. Dance, E. Climent, and M.R. Maxey (unpublished).
[26] J.R. Taylor, *An Introduction to Error Analysis* (Oxford University Press, Oxford, 1982).
[27] H. Nicolai, B. Herzhaft, E.J. Hinch, L. Oger, and E. Guazzelli, Phys. Fluids **7**, 3 (1995).
[28] J.F. Richardson and W.N. Zaki, Trans. Inst. Chem. Eng. **32**, 35 (1954).
[29] E. Guazzelli, Phys. Fluids **13**, 1537 (2001).
[30] J.Z. Xue, E. Herbolzheimer, M.A. Rutgers, W.B. Russel, and P.M. Chaikin, Phys. Rev. Lett. **69**, 1715 (1992).
[31] X. Lei, B.J. Ackerson, and P. Tong, Phys. Rev. Lett. **86**, 3300 (2001).
[32] B. Cichocki, R.B. Jones, R. Kutteh, and E. Wajnryb, J. Chem. Phys. **112**, 2548 (2000).
[33] D. Bruneau, F. Feuillebois, R. Anthore, and E.J. Hinch, Phys. Fluids **8**, 2236 (1996).
[34] D. Leighton and A. Acrivos, Chem. Eng. Sci. **41**, 1377 (1986).
[35] G.E. Karniadakis and S.J. Sherwin, *Spectral/hp Element Methods for CFD* (Oxford University Press, Oxford, 1999).
[36] V. Girault and P.A. Raviart, *Finite Element Methods for Navier-Stokes Equations: Theory and Algorithms* (Springer-Verlag, New York, 1986).
[37] E.M. Rønquist, Ph.D. thesis, MIT, 1988.
[38] C. Canuto, *Spectral Methods in Fluid Dynamics* (Springer-Verlag, New York, 1988).
[39] Y. Maday, D. Meiron, A.T. Patera, and E.M. Rønquist, SIAM J. Sci. Comput. (USA) **14**, 310 (1993).
[40] S.L. Dance, Ph.D. thesis, Brown University, 2002.